LAWRENCE
LIVERMORE
NATIONAL
LABORATORY

LLNL-JRNL-761383

Intrinsic Shape of Free Carrier Absorption Spectra in 4H-SiC

P. Grivickas, K. Redeckas, K. Gulbinas, A. Conway, L. Voss, M. Bora, S. Sampayan, M. Vengris, V. Grivickas

November 12, 2018

Journal of Applied Physics

Disclaimer

Intrinsic Shape of Free Carrier Absorption Spectra in 4H-SiC

P. Grivickas[1*], K. Redeckas[2], K. Gulbinas[3], A. M. Conway[1], L. F. Voss[1], M. Bora[1], S. Sampayan[1], M. Vengris[2], and V. Grivickas[3]

[1]Lawrence Livermore National Laboratory, 7000 East Avenue, Livermore, California 94550, USA
[2]Laser Research Center, Vilnius University, Sauletekio avenue 10, Vilnius, LT-10223, Lithuania
[3]Institute of Photonics and Nanotechnology, Vilnius University, Sauletekio avenue 3, Vilnius, LT-10257, Lithuania

Abstract
Free carrier absorption spectra are measured along the different polarization directions with respect to the *c*-axis of 4H-SiC using ultrafast differential transmission spectroscopy. Probing of excited carrier spectra in undoped material reveals intrinsic resonances within the conduction band. Widths of the detected resonance peaks are shown to be wider than their theoretical estimates and more comparable to the ones observed in low doped material. Relative strength of the peaks on the other hand is shown to be nearly excitation independent in contrast to the doping induced absorption weakening for the same transitions in *n*-type samples. Free carrier cross-sections are extracted from the excitation dependency of the detected spectra and linked to the individual electron and hole contributions in the near infrared range.

[*] Email of the corresponding author: grivickas1@llnl.gov

Introduction

Free carrier absorption (FCA) has been a subject of extensive studies over the years due to its practical importance for non-destructive evaluation of doping in semiconductors. Several theoretical frameworks based on specific band structures and different carrier scattering mechanisms were proposed to describe the phenomenon [1-3]. Appropriate parametrization strategies based on these frameworks are still being developed and debated even for Si [4-6]. The next strong impetus for FCA investigation came with the advancement of the pump-probe technique for monitoring carrier dynamic processes in excited semiconductors [7]. Carrier lifetimes, surface recombination rates, diffusion coefficients and dynamic mechanisms underlying these parameters were extracted from FCA transients in Si [8-10], InN [11], GaN [12], CdTe [13], diamond [14], SiC [15-17] and many other semiconductors.

The classical Drude model predicts a quadratic wavelength dependency of FCA when photon energies exceed the plasma frequency [18,19]. This dependency can be perturbed significantly by resonant inter-conduction band transitions. A clear example of such transitions is the case of non-cubic polytypes of SiC where the zone folding effect at the periodic twin-boundaries results in multiple bands. The resonant transitions between such bands manifest themselves as absorption peaks sometimes referred to as the Biedermann bands [20], or optical resonances (ORs) [21-23], and serve as a distinct spectral fingerprint for each polytype [24-26]. Spectral position, shape and polarization dependency of ORs have been instrumental in developing a comprehensive picture of electronic structure evolution in SiC polytypes with different stacking sequences [27].

Details about the OR peaks in 4H-SiC have been obtained exclusively from *n*-type doped samples using standard optical transmission (TR) measurements. Such spectra are inevitably perturbed by shifting, broadening and convolution effects induced by shallow impurity states. This raises questions about separating the intrinsic shape of the OR peaks within the conduction band from the contribution of the donor state. Pump-probe measurements provide information about the intrinsic transitions if excited carriers are thermally relaxed to the bottom of the conduction band. In 4H-SiC, however, the pump-probe approach has been limited to calibration of FCA cross-sections at a few probing wavelengths in the infrared range [22,28]. In this work, we extend excited carrier detection over a continuous 400 – 1000 nm wavelength range in order to reveal ORs along the two principal polarizations (parallel and perpendicular) with respect to the hexagonal *c*-axis in 4H-SiC. Measurements are done by using ultrafast differential transmission spectroscopy (UDTS) based on broad continuum probing. Sub picosecond resolution of the technique allows monitoring instantaneous carrier concentration even in a material with a short carrier lifetime. By comparing the spectra of doped and undoped samples detected using the same method we deduce the shape and magnitude of the intrinsic ORs in this material and provide calibration of the FCA cross-section over a broad spectral range.

Experimental method

Experiments were performed on three samples with concentrations of N donors and Al and B acceptors summarized in Table I from Secondary Ion Mass Spectroscopy (SIMS) measurements. The undoped (UN) sample was sectioned from a free-standing high-quality epilayer of 250 μm thickness. The epilayer was grown by a high temperature chemical vapor deposition on an 8.5^{o} off axis substrate. The doped samples were cut from *n*- and *p*-type substrates grown by physical vapor deposition and had similar thickness as the UN sample. Fig. 1 shows the schematics of experiments with the pump and probe beams being almost collinear with respect to each other (< 2^{o} angle) and normal to the probed surface. The *c*-axis was parallel to the probed surface. The pump beam was always kept $E \perp c$ polarized while the polarization of the probe beam was either $E \perp c$ or $E \| c$. The two beams were overlapped with the ~60 μm diameter probe being positioned within the ~100 μm diameter pump. Both beams originated from the same Ti-Sapphire laser (Coherent Libra-USP) generating 50 fs duration pulses at 800 nm wavelength. Part of the fundamental output was used to generate pump light at 355 nm using an optical parametric amplifier (Topas-800, Light Conversion) while the remaining part was used to generate a white light continuum in a sapphire crystal and served as a probe. The 680 – 830 nm (1.5 -1.8 eV) range of the 400 - 1000 nm continuous probe spectrum was blocked by a notch filter to avoid the 800 nm excitation wavelength.

Differential transmission (DT) of the probe beam at each wavelength is defined as the I/I_0 ratio, where I_0 and I are the intensities of the probe beam before and after the arrival of the excitation pulse. In both cases the signal is detected behind a sample by a spectrometer and a diode array. In our experiments, $\log(I/I_0)$ is expressed in the relative units of optical density (o.d.) and related to excited carrier FCA according to:

$$\log\left(\frac{I_0}{I}\right) = \frac{1}{\ln(10)}\int_0^d \Delta\alpha_{FCA}(x)dx, \tag{1}$$

$$\Delta\alpha_{FCA}(x) = \sigma_n \Delta n(x) + \sigma_p \Delta p(x), \tag{2}$$

$$\Delta n(x) = \Delta p(x) = \Delta n(x=0)\exp(-\alpha_{BB}x) = \frac{(1-R)E\alpha_{BB}}{A\hbar\omega}\exp(-\alpha_{BB}x), \tag{3}$$

where $\Delta\alpha_{FCA}$ is the FCA absorption coefficient, σ_n and σ_p are the FCA cross-sections of free electrons and holes, respectively, α_{BB} = 200 cm^{-1} is the band-to-band absorption coefficient at 355 nm for the $E\perp c$ polarization [29], d is the sample thickness along the probe direction, R = 0.22 is the reflectivity of SiC in the considered spectral range [30], E is the energy of the excitation pulse, A is the area of the pump beam, and $\hbar\omega$ = 3.49 eV is the photon energy. It is evident from Eq. (3) that the probe is not sampling a uniform carrier concentration but rather a profile. To account for the exponential distribution in the sample we relate the DT signal to the following average parameters which are obtained after the substitution of Eqs. (2) and (3) into Eq. (1) and the subsequent integration:

$$\frac{\ln(10)}{d}\log\left(\frac{I_0}{I}\right) = \Delta\alpha_{AV} = \sigma\Delta n_{AV}, \tag{4}$$

$$\Delta n_{AV} = \frac{\Delta n(x=0)}{\alpha_{BB}d}\left(1-\exp(-\alpha_{BB}d)\right) = \frac{(1-R)E}{dA\hbar\omega}\left(1-\exp(-\alpha_{BB}d)\right), \tag{5}$$

where σ depends on the carrier type. Eq. (5) describes carrier concentration of an instantaneous excited state unaffected by carrier recombination and diffusion processes. The inset of Fig. 1 demonstrates that the fastest decay with the sub 10 ns carrier lifetime was detected in the doped 4H-SiC substrate. Even such a short time scale is much longer than the pulse duration used in current experiments. Thermal equilibration of excited carriers was achieved by using a 10 ps delay between the pump and the probe.

Results and discussion

Fig. 2 (a) shows DT spectra (red and blue lines) detected in the UN 4H-SiC at the excitation level of $\Delta n_{AV} = 4\times10^{17}$ cm^{-3} for the two principal polarizations. The data are compared to the spectra obtained by TR in *n*-type samples with three different dopings (gray curves with different styles): The relatively low-doped (LD) ~ 5×10^{17} cm^{-3} samples [21], the moderately-doped (MD) substrate used in this work (Table I) and the highly-doped (HD) > 1×10^{19} cm^{-3} samples [20]. All spectra are normalized with respect to the prominent OR peaks around 2.08 eV for E||c and 2.66 eV for E⊥c. The origin of the OR peaks is explained in Fig. 2 (b) using the calculated electronic structure of the conduction band near the indirect band-gap of 4H-SiC at the M symmetry point [27]. Several bands, labeled as c2 – c5, emerge above the lowest c1 band due to the folding effect at the boundaries of the Brillouin zone. They have one of the two symmetry characteristics as represented by the solid and dashed lines. Selection rules dictate that optical transitions are allowed between the bands of the same symmetry for the E||c polarization (blue arrows) and between the bands of the different symmetry for the E⊥c polarization (red arrows) [26,27]. According to the diagram, the prominent OR peaks correspond to the transitions from the lowest energy state in the c1 band (solid vertical arrows). Alternative transitions from the higher in energy c2 band are indicated by the dashed arrows. Expected peak positions are indicated by the correspondingly labeled arrows in Fig. 2 (a).

The DT spectra in the excited UN sample are comparable to the steady state absorption in the LD sample. The two samples have similar concentration of electrons but the concentration of N donors in the UN sample is two orders of magnitude lower as compared to the LD sample. The role of the N donor state in optical transitions is illustrated schematically in Fig. 2 (b) by the green line. In 4H-SiC, the N level lie below the conduction band minimum by 45 - 65 meV and 105 -125 meV for the hexagonal and cubic sites, respectively [31]. These energies are much larger than the thermal energy of electrons at room temperature and suggest optical transitions originating from the N state directly. The N state has a delocalized nature in *k*-space resulting in partial relaxation of the $\Delta k = 0$ selection rule for vertical transitions leading to broadening of the OR peaks [27]. In the UN sample, excited carriers instead relax to the bottom of the c1 band and should be exclusively described by the inter-conduction band transitions. Estimates of the intrinsic OR widths were done using Boltzmann statistics and the calculated density of states in 4H-SiC [27]. The estimated OR peak shapes are reproduced in Fig. 2 (a) by the black curves (labeled EST) with the corresponding full width half maximum (FWHM) values of 55 meV and 30 meV for the A1 and B1 transitions, respectively. The experimentally measured OR peaks are several times wider than these theoretical predictions.

To make sure that the width of the measured OR peaks is representative of intrinsic transitions and does not dependent on excited carrier concentration, we perform detailed analysis of the DT spectra in Fig. 3. Fig. 3 (a) shows the shape of the OR peak for the E||c polarization at different excitations. With decreasing carrier concentration, the peak narrows predominantly on the low energy side. We reproduced the effect by using two Gaussian peaks with the same FWHM as shown in Fig. 3 (a) by the dashed and dashed-dotted lines. The separation between the small and the large peaks remain constant at 115±10 meV for all excitation conditions while the relative amplitude of the smaller peak decreases with decreasing excitation. The FWHM and center of the overall OR fits are reproduced by the blue symbols in Fig. 3 (b) and (c) for the entire excitation range. The obtained parameter changes are guided by polynomial fits (solid curves) showing convergence of FWHM at low excitation conditions to 185±5 meV for E||c. The same analysis was repeated for the E⊥c peak using 90±10 meV separation between the Gaussian peaks. FWHM saturation (red symbols with corresponding fits) was observed at 140±5 meV.

Broadening of the excited OR peaks predominately on the low energy side with increasing excitation contrasts with broadening of the doped TR peaks. In the latter case, it occurs as a skew on the high energy side with increasing doping concentration, best seen in Fig. 2 (a) for the E⊥c peak. Such behavior has been observed for both 4H- and 6H-SiC polytypes [23-26] and attributed to the Fano-type resonance between the N state and the high energy bands [25]. The Fano analysis is applicable for both LD and MD samples while in the HD samples the broadening is dominated by such phenomena as the Mott transition, band tailing, and band-gap narrowing [27]. In the excited UN sample, broadening on the low energy side persists up to the highest excitations probed indicating a probable onset of new interactions. One of the tentative explanations can be an involvement of a transition from the c2 band. The c2 band is estimated to be 144 meV above the c1 band [32] in agreement with the obtained separation between the two Gaussian fitting peaks. Population of the c2 band, however, cannot be justified using just Boltzmann statistics.

DT changes in the whole excitation range are shown in Fig. 3 (d) for two specific regions (energies indicated in the figure): at the tip of the OR peak (circle symbols) and at the energy outside the OR peak (square symbols) for both polarizations (red and blue colors). All data are fitted using the linear FCA dependence inferred by Eq (4) as shown by the solid lines. Small deviations from the linear dependence are only noticeable at the excitations above ~5×10^{17} cm^{-3} and are most likely related to the OR peak broadening documented in Fig. 3 (a). Constant difference between the two regions in each polarization indicates that the amplitude of the excited OR peaks is almost independent of excess carrier concentration. This finding contrasts with clear reduction of the OR peaks relative to the absorption background with increasing doping concentration as seen from the gray curves in Fig. 2 (a). It is not clear, however, if the result is caused by the decrease in resonance amplitude or by the increase in spectral background with respect to the excited case since all spectra in the figure are plotted on the relative scale. To separate the two effects, all spectra were quantified by converting them into cross-section units.

In the excited UN sample, the $\sigma \approx \sigma_n$ fitting parameter was estimated at the tip of the OR peaks since it is dominated by the conduction band transitions there, and subsequently used to scale the DT spectra. The results for the two polarizations are shown by the red lines in Fig. 4. In the doped *n*-type MD sample, the same parameter was obtained from the $\sigma_n = \alpha_{FCA} / N_D$ relation, where N_D stands for the nitrogen concentration, approximated by the SIMS values in Table I. The obtained cross-sections are shown by the black lines in Fig. 4. For both polarizations, the OR peak height of the excited UN sample clearly exceeds that observed by TR in the MD sample by a factor of four, while in both cases cross-section magnitudes match reasonably outside the OR region. The same finding was independently confirmed by implementing UDTS measurements and cross-section calibration in the MD sample itself under the $\Delta n = \Delta p \cong N_D$ excitation condition. The result is shown in Fig. 4 by the blue curves and closely matches the TR absorption spectra. Finally, UDTS measurements were carried out in the *p*-substrate where Al acceptors should have no effect on the ORs in the conduction band. The result is shown in Fig. 4 by the green curves. In this case, the obtained DT spectra closely match the ones in the excited UN sample, corroborating that the strength of the OR peaks is only affected by the presence of N donor states.

Fig. 4 also compares our data with the previously reported FCA cross-sections in UN 4H-SiC using pump-probe measurements at specific excitation wavelengths in the infrared region [22,28], as shown by the red symbols. For both polarizations, good agreement can be seen in the overlapping regions at 1.4 eV and 2 eV. At lower energies, the literature data follow the same trend as the TR data from the *n*-substrate but are substantially higher in magnitude. We fit both cases using the same λ^2 ($\lambda^{2.5}$) dependency for the $E\|c$ ($E\perp c$) polarization as shown by the dash-dotted and the dashed curves, respectively. The obtained dependences are consistent with the lambda square law predicted by the classical Drude model. The difference between the two curves (short-dashed curves) was attributed to σ_p since $\sigma = \sigma_n + \sigma_p$ in the excited UN sample according Eq. (2) while $\sigma = \sigma_n$ in the *n*-substrate. Such unambiguous assignment of the σ_p parameter is confirmed by the earlier discussed matching of all spectra in the OR region.

Conclusion

We show that the intrinsic shapes of OR in FCA spectra extracted in the excited UN material using UDTS measurements are different from the ones reported by TR measurements in doped *n*-type 4H-SiC samples. Specifically, we see that the OR peaks reverse in their shape asymmetry and increase in strength by a factor of four. These changes are in line with the expected strengthening of quantum mechanical coupling due to elimination of N donor states. On the other hand, the lack of OR peak narrowing at the lowest excitation conditions contrasts with theoretical predictions using the calculated electronic structure of 4H-SiC. This suggests partial relaxation of the selection rules even in undoped material. FCA cross sections extracted in this work provide the first reliable platform for comparison of carrier concentrations in different types of experiments. We show that the extracted contribution of free holes exceeds the one of free electrons in the infrared region of 4H-SiC by a factor of four while following similar spectral dependency predicted by the Drude model. This opens possibilities to distinguish free electrons and holes from charged Al acceptor states in photo-induced absorption measurements in *p*-type material [33].

Auspices

V. G. wishes to thank the Research Council of Lithuania for the support of the LB-17-01 grant named "Transient optical processes in compensated silicon carbide and chalcogenide 2D semiconductors". M.V. was funded by the European Regional Development Fund according to the supported activity "Research Projects Implemented by World-class Researcher Groups" under measure No. 01.2.2-LMT-K-718, grant No. 01.2.2-LMT-K-718-01-0014. This work was performed under the auspices of the U.S. Department of Energy by Lawrence Livermore National Laboratory under Contract DE-AC52-07NA27344 and was supported by the LLNL-LDRD program under project No. 17-ERD-050.

References

[1] B. Jensen, Annals of Physics **80**, 284 (1973).
[2] R. Sirko and D. L. Mills, Phys. Rev. B **18**, 5637 (1978).
[3] I. Kleinert and M. Giehler, Phys. Stat. Sol. (b) **136**, 763 (1986).6
[4] J. Isenberg, and W. Warta, Appl. Phys. Lett. **84**, 2265 (2004).
[5] M. Rudiger, J. Greulich, A. Richter, and M. Hermle, IEEE Tr. on El. Dev. **60**, 2156 (2013).
[6] S. C. Baker-Finch, K. R. McIntosh, D. Yan, K. C. Fong, and T. C. Kho, J. of Appl. Phys. **116**, 063106 (2014).
[7] J. Linnros, J. of Appl. Phys. **84**, 275 (1998).
[8] V. Grivickas, and J. Linnros, Appl. Phys. Lett. **59**, 72 (1991).
[9] J. Meitzner, F. G. Moore, B. M. Tillotson, S. D. Kevan, and G. L. Richmond, Appl. Phys. Lett. **103**, 092101 (2013).
[10] S. C. Siah, M. T. Winkler, D. M. Powell, S. W. Johnston, A. Kanevce, D. H. Levi, and T. Buonassisi, J. of Appl. Phys **117**, 105701 (2015).
[11] S. Nargelas, R. Aleksiejunas, M. Vengris, T. Malinauskas, K. Jarasiunas, and E. Dimakis, Appl. Phys. Lett. **95**, 162103 (2009).
[12] P. Scajev, K. Jarasinas, U. Ozgur, H. Morkoc, J. Leach, and T. Paskova, Appl Phys. Lett. **100**, 022112 (2012).
[13] P. Scajev, S. Miasojedovas, A. Mekys, D. Kuciauskas, K. G. Lynn, S. K. Swain, and K. Jarasiunas, J. of Appl. Phys **123**, 025704 (2018).
[14] P. Scajev, Physica B **510**, 92 (2017).
[15] A. Galeckas, J. Linnros, V. Grivickas, U. Lindefelt, and C. Hallin, Appl. Phys. Lett. **71,** 3269 (1997).
[16] A. Galeckas, V. Grivickas, J. Linnros, H. Bleichner, and C. Hallin, J. of Appl. Phys. **81**, 3522 (1997).
[17] A. Galeckas, J. Linnros, M. Frischholz, and V. Grivickas, Appl. Phys. Lett. **79,** 365 (2001).
[18] J. I. Pankove, *Optical Processes in Semiconductors*, (Prentice-Hall, Inc. NJ, 1971).
[19] B. K. Ridley, *Quantum Processes in Semiconductors*, (Clarendon Press, Oxford, 1993).
[20] E. Biedermann, Sol. St. Commun. **3**, 343 (1965).
[21] S. G. Sridhara, S. Bai, O. Shigiltchoff, R. P. Devaty, and W. J. Choyke, Mat. Sci. Forum **338-342**, 551 (2000).
[22] V. Grivickas, A. Galeckas, P. Grivickas, and J. Linnros, Mat. Sci. Forum **338-342**, 555 (2000).
[23] E. Weingartner, P. J. Wellmann, M. Bickermann, D. Hofmann, and T. L. Straubinger, Appl. Phys. Lett. **80**, 70 (2002).
[24] B. Ellis and T. S. Moss, Proc. Royal Soc. A **299**, 393 (1967).
[25] R. Weingartner, M. Bickermann, Z. Herro, U. Kunecke, S. A. Sakwe, P. J. Wellmann, and A. Winnacker, Mat. Sci. Forum **433-436**, 333 (2003).
[26] W. J. Choyke, H. Matsunami, and G. Pensl, *Silicon Carbide*, (p. 418, Springer, 2004).
[27] S. Limpijumnong, W. R. L. Lambrecht, S. N. Rashkeev, and B. Segall, Phys. Rev. B 59 (1999) 12890.
[28] P. Ščajev and K. Jarašiūnas, J. Phys. D: Appl. Phys. **46**, 265304 (2013).
[29] A. Galeckas, V. Grivickas, V. Bikbajevas, J. Linnros, and P. Grivickas, Phys. Stat. Sol. A **191** 613 (2002).
[30] A. M. Ismail, and H. Abu-Safia, J. of Appl. Phys. **91**, 4114 (2002).
[31] T. Kimoto, A. Itoh, H. Matsunami, S. Sridhara, L. L. Clemen, R. P. Devaty, W. J. Choyke, T. Dalibor, C. Peppermuller, and G. Pensl, Appl. Phys. Lett. **67,** 2833 (1995).
[32] W. Klahold, C. Tabachnick, G. Freedman, R. P. Devaty, and W. J. Choyke, Mat. Sci. Forum **897**, 250 (2017).
[33] G. Liaudanskas, P. Scajev, and K. Jarasiunas, Semicon. Sci. Technol. **29,** 015004 (2014).

Tables

Sample	N	Al	B
Epilayer (UN)	1.5e15 cm^{-3}	< 1e15 cm^{-3}	< 1e15 cm^{-3}
n-substrate (MD)	3.3e18 cm^{-3}	< 2e14 cm^{-3}	1.4e15 cm^{-3}
p-substrate (MD)	1.9e15 cm^{-3}	4.5e18 cm^{-3}	< 7e14 cm^{-3}

Table I Doping concentrations in different samples from SIMS (UN – undoped, MD – moderately doped).

Figure captions

Fig. 1 Schematic representation of UDTS measurements (left) and example of a detected carrier decay (right).

Fig 2. (a) Normalized FCA spectra in excited undoped 4H-SiC (blue and red curves) in comparison to the optical transmission data in *n*-type 4H-SiC with different dopings (grey curves) and theoretical estimates (black curves). (b) Electronic structure of the conduction band in 4H-SiC [27] with the allowed transitions for the two light polarizations (arrows).

Fig 3. (a) Normalized OR peaks at the E||c polarization in undoped 4H-SiC for different excitation levels (symbols) and their fits (solid lines) using two Gaussian peaks (dashed and dashed-dotted lines). Peak center energy positions (b) and FWHM (c) extracted from the data analysis for two polarizations. (d) DT signal at the tip of the OR peak (circle symbols) and at the energy outside the OR peak (square symbols) versus the excited carrier concentration for two polarizations. Linear fits are shown by the lines.

Fig 4. FCA cross-sections in 4H-SiC for two light polarizations. Colored curves are DT spectra extracted in the excited UN sample (red), the MD *n*-substrate (blue) and the MD *p*-substrate (green). The black curve is the TR data in the MD n-substrate. Square [22] and circle [28] symbols are pump-probe data measured using specific laser wavelengths in UN grade 4H-SiC. Dashed and dashed-dotted curves are fits using $\sigma = \sigma_n$ and $\sigma = \sigma_n + \sigma_p$ approximations. The short-dashed curve is the difference of the two fits representing the $\sigma = \sigma_p$ dependence.

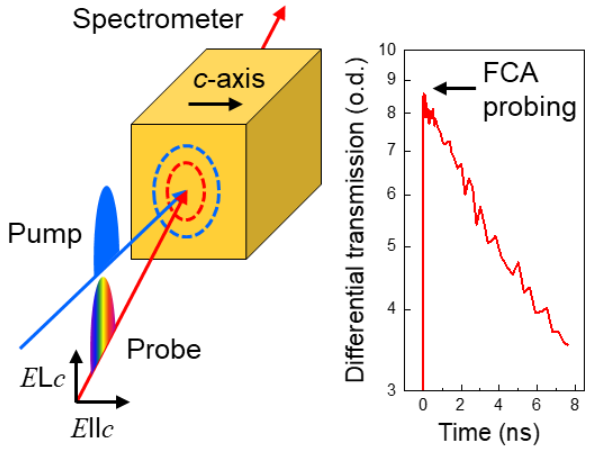
Spectrometer
c-axis
Pump
Probe
ELc
EIIc
Differential transmission (o.d.)
FCA
probing
Time (ns)
10
9
8
7
6
5
4
3
0
2
4
6
8

Fig. 1

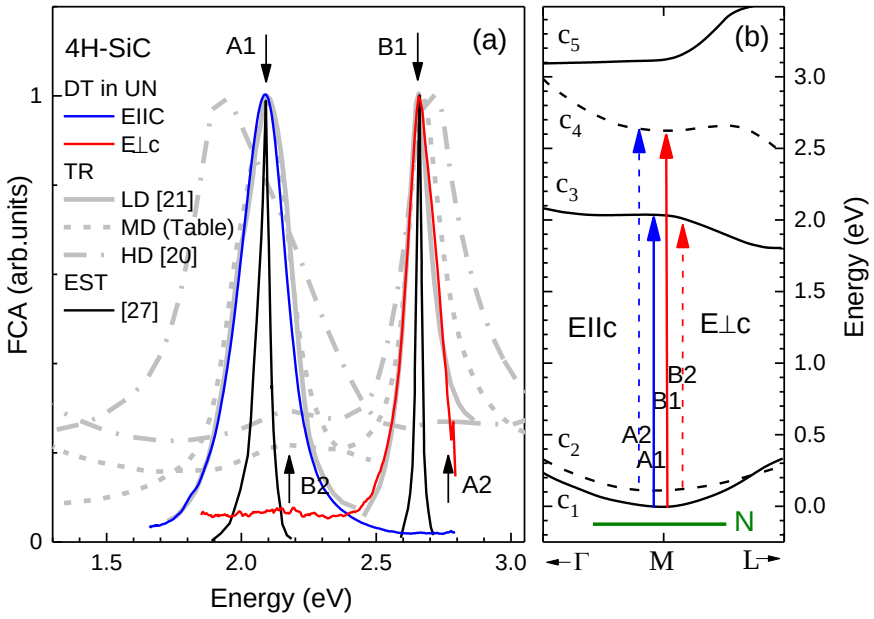
4H-SiC
DT in UN
EIIC
E⊥c
TR
LD [21]
MD (Table)
HD [20]
EST
[27]
A1
B1
B2
A2
(a)
FCA (arb.units)
Energy (eV)
(b)
c5
c4
c3
c2
c1
EIIc
E⊥c
B2
B1
A2
A1
N
←Γ
M
L→
Energy (eV)

Fig 2.

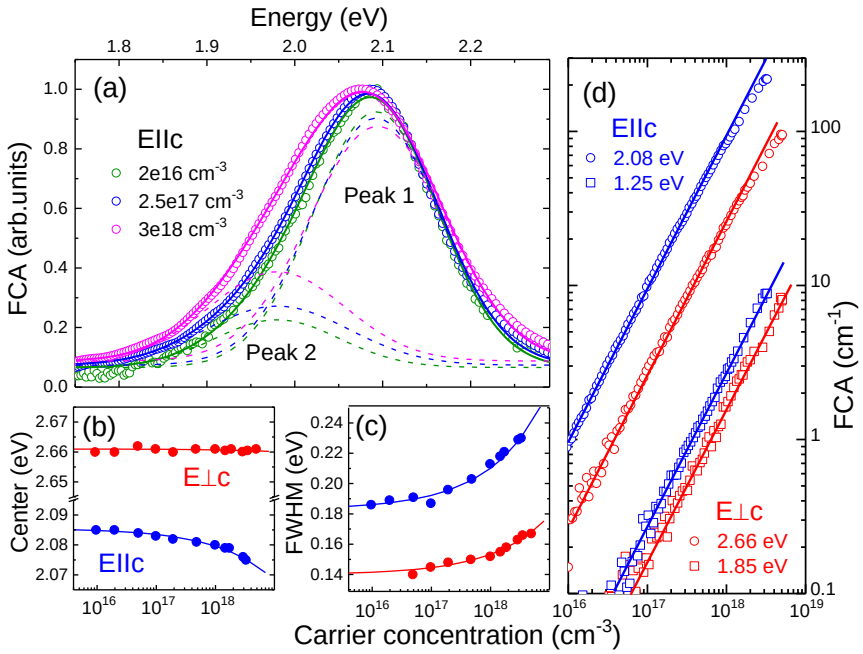
Energy (eV)
1.8
1.9
2.0
2.1
2.2
(a)
EIIc
2e16 cm-3
2.5e17 cm-3
3e18 cm-3
Peak 1
Peak 2
FCA (arb.units)
1.0
0.8
0.6
0.4
0.2
0.0
(b)
E⊥c
EIIc
Center (eV)
2.67
2.66
2.65
2.09
2.08
2.07
(c)
FWHM (eV)
0.24
0.22
0.20
0.18
0.16
0.14
(d)
EIIc
2.08 eV
1.25 eV
E⊥c
2.66 eV
1.85 eV
FCA (cm-1)
100
10
1
0.1
10^16
10^17
10^18
10^19
Carrier concentration (cm-3)

Fig 3.

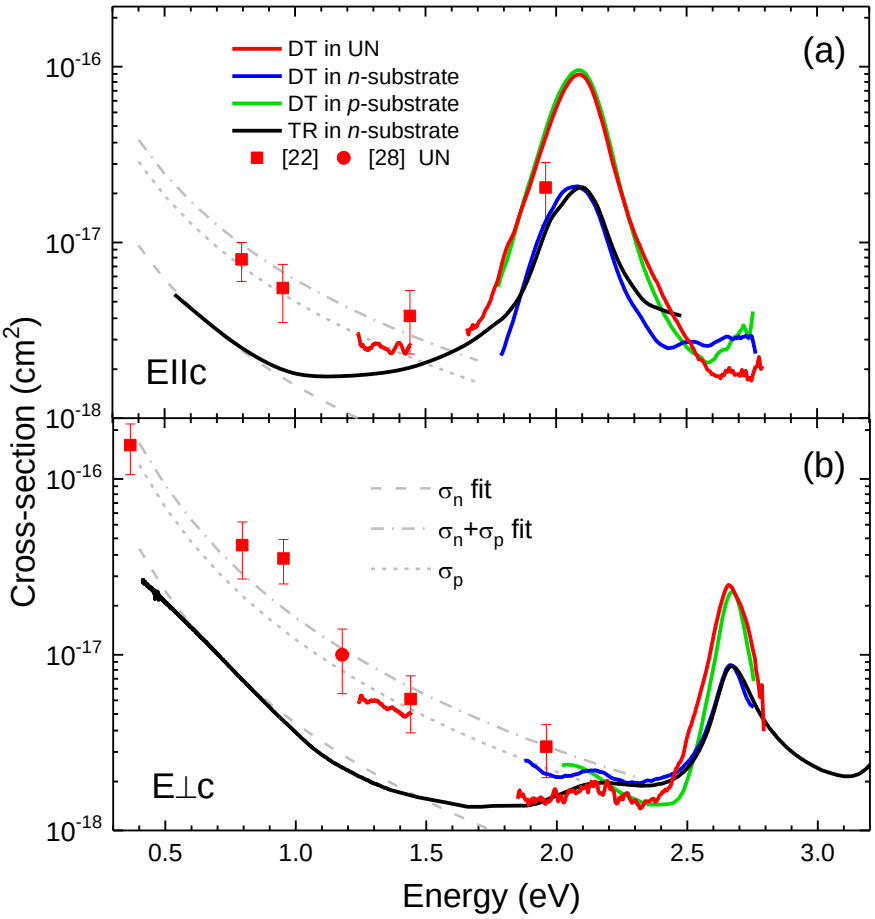
DT in UN
DT in n-substrate
DT in p-substrate
TR in n-substrate
[22] [28] UN
(a)
EIIc
(b)
σn fit
σn+σp fit
σp
E⊥c
Cross-section (cm2)
Energy (eV)
10-16
10-17
10-18
0.5
1.0
1.5
2.0
2.5
3.0

Fig 4.